

Modernization of the DCHAIN-PHITS activation code with new features and updated data libraries

Hunter N. Ratliff^{a,*}, Norihiro Matsuda^a, Shin-ichiro Abe^a, Takamitsu Miura^b, Takuya Furuta^a, Yosuke Iwamoto^a, Tatsuhiko Sato^a

^aJapan Atomic Energy Agency (JAEA), 2-4 Shirakata, Tokai, Naka, Ibaraki 319-1195, Japan

^bResearch Organization for Information Science and Technology (RIST), 2-4 Shirakata, Tokai, Naka, Ibaraki 319-1106, Japan

Abstract

Induced radioactivity is critical in a variety of fields including maintenance and decommissioning of accelerators and reactors, nuclear waste management, and radionuclide production for medical and industrial applications. Serving this purpose, DCHAIN-PHITS is the time-dependent radionuclide production, buildup, burnup, and decay code which is coupled to and distributed with the PHITS general purpose Monte Carlo particle transport code. While the core of the DCHAIN code was first written over forty years ago, the DCHAIN-PHITS incarnation of the code represents its most substantial update in nearly twenty years. This work provides an overview of the function of DCHAIN-PHITS and the new additions to the code. These additions include updated decay and cross section nuclear data libraries, statistical uncertainty propagation, support for tetrahedral and three-dimensional grid mesh geometries, reaction tracking capabilities, and general performance improvements.

Keywords: activation, decay, burnup, induced activity, PHITS

1. Introduction

DCHAIN [1, 2] is a decay chain analysis code for simulating the production, buildup, burnup, and decay of nuclides as a function of time in any radiation environment, specifically designed with accelerator facilities in mind. It is coupled to and distributed alongside the PHITS (Particle and Heavy Ion Transport code System) general purpose Monte Carlo particle transport code [3]; PHITS serves as DCHAIN's source for neutron flux spectra and nuclide production through complex high-energy nuclear reactions for which the physics models within PHITS are employed. PHITS can model nearly any particle (photons, leptons, mesons, baryons, and ions) and its radionuclide-producing reactions over a large range of energies (meV~TeV). Briefly put, PHITS performs the time-independent (relative to activation time scales) calculations such as particle transport and nuclear reactions. Then, DCHAIN assembles time-dependent decay/reaction chains and propagates nuclide inventories through time provided the nuclear reaction rates and neutron fluxes from PHITS and the power schedule of the source/beam, ultimately outputting time-dependent nuclide inventories, decay heats, photon spectra, and effective dose rates. DCHAIN-PHITS, referred to as just DCHAIN for brevity, is an upgraded and modernized version of the DCHAIN-SP code [2].

This update to DCHAIN provides a number of new data libraries and features discussed in detail throughout this paper, summarized here. Two decay data libraries and ten neutron reaction cross section libraries (along with several hybrid combinations of each type) have been added to DCHAIN, now allowing for the user to select their libraries of choice and perform comparative calculations. A new output file illustrating the constructed decay/reaction chains and allowing for much more detailed tracking of nuclide inventories throughout a simulation has also been implemented. This new output file can explicitly describe how much each specific reaction contributes to the inventory of a nuclide and could be used to greatly benefit efforts in designing or selecting materials to minimize activation.

Prior to this work, the statistical uncertainties from the PHITS-calculated nuclear reaction nuclide yields and neutron fluxes were not propagated through the DCHAIN calculations; this has been addressed with DCHAIN now propagating these uncertainties and reporting their influence on the results. Though this functionality is also present in “all-in-one” codes such as FLUKA [4], it is unique among the other widespread and more traditional modularly-coupled codes [5] such as the MCNP particle transport code [6] with the CINDER [7] or ORIGEN [8] transmutation and burnup codes.

Support for three-dimensional grid mesh and tetrahedral geometries has been added along with some optimizations for geometries with many regions. Special features of note here include that the voxels within a 3-D grid mesh geometry can contain an arbitrary number of mate-

*Corresponding author.

Email address: ratliff.hunter@jaea.go.jp (H. N. Ratliff)

rial boundaries (no per-voxel homogeneity constraint) and that tetrahedral problems can output files formatted to enable coupling to the FLUENT [9] computational thermal and fluid dynamics software, allowing DCHAIN-calculated decay heats to be used directly as a heating source term in those simulations. Both of these newly supported geometry types also provide capabilities for determining spatial distributions of activation with far higher fidelity than available with more traditionally defined geometries.

The history, mathematical theory, and usage principles of DCHAIN are discussed next in Section 2. Section 3 then reviews the new decay and cross section data library additions and improvements. Section 4 presents the newly implemented features and capabilities of the DCHAIN code, and these new features and updated libraries are showcased in example calculations in Section 5.

2. History, theory, and usage of DCHAIN

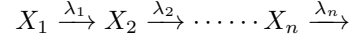
2.1. A brief history of the DCHAIN code

DCHAIN was first released by Tasaka in 1977 [10], and he later released DCHAIN2 with numerous feature improvements and additions in 1980 [1]. In 1999, DCHAIN-SP was released [11] with a new focus placed on spallation products. In 2001, DCHAIN-SP 2001 was released which featured specific data library improvements for the needs of the J-PARC accelerator facility [2]; this is the most recent “substantial” release of DCHAIN. In the following year, a report on the reliability of DCHAIN-SP 2001 was published [12]. In 2009, the FENDL/A-2.0 [13] neutron reaction cross section library within DCHAIN was replaced with the JEFF-3.1A library [14], and the cross section energy group structure was upgraded from the VITAMIN-J 175-group structure [15] to the ECCO 1968-group structure [16]. This update was not published in a report but was instead presented at a conference in 2009 [17].

First coupling DCHAIN-SP 2001 to PHITS, the tally [T-Dchain] was implemented in PHITS version 2.52 in late 2012; in early 2015 with the release of PHITS 2.75, this was updated to the 2009 version of DCHAIN-SP. Some of the features presented in this work were made available with the release of PHITS 3.14 in 2019, with a few appearing slightly earlier; from this update the official name of the DCHAIN code became DCHAIN-PHITS with a version number matching that of the PHITS code with each release. All of the features discussed within this work are available in DCHAIN-PHITS version 3.21 (released in 2020) and onward.

2.2. Theory and principles

DCHAIN employs the Bateman method for determining the time-dependent production, buildup, and decay of nuclides [18]. Bateman’s general solution is for a decay chain of arbitrary length such as the one illustrated below where X_i is a radioactive nuclide with decay constant λ_i and the final nuclide X_n may be stable with $\lambda_n = 0$.



Nuclide inventories within DCHAIN are influenced by three mechanisms: decay, neutron reactions under 20 MeV, and source-target plus all other nuclear interactions (separate from the low-energy neutron reactions). As described by Tasaka [1], the change in inventory of a nuclide i with time can be expressed with Equation 1.

$$\begin{aligned} \frac{dN_i(t)}{dt} = & Y_i(t) - (\lambda_i + \sigma_{\text{tr},i}\phi(t))N_i(t) \\ & + \left(\sum_j f_{j \rightarrow i} \lambda_j N_j(t) \right) + \left(\sum_k g_{k \rightarrow i} \sigma_{\text{tr},k} \phi(t) N_k(t) \right) \end{aligned} \quad (1)$$

where:

$N_i(t)$ = inventory of nuclide i at time t

$Y_i(t)$ = production rate of nuclide i through source-target and other nuclear interactions at time t

λ_i = decay constant of nuclide i

$\sigma_{\text{tr},i}$ = flux-weighted total microscopic neutron transmutation reaction cross section of nuclide i

$\phi(t)$ = total neutron flux at time t

$f_{j \rightarrow i}$ = branching ratio of the decay of nuclide j to nuclide i

$g_{k \rightarrow i}$ = fractional production probability of nuclide i per transmuting neutron reaction with nuclide k

In the most basic form of Bateman’s solution, it is assumed that only the first nuclide in a chain has nonzero initial inventory. The more general solution where all nuclides in a chain may begin with nonzero inventories is found by superimposing the basic solution for i linear decay chains of lengths i to 1 and initial nuclide inventories of N_1^0 to N_i^0 . Neglecting the neutron reaction term momentarily ($\phi = 0$), this general solution to Equation 1 is shown in Equation 2.

$$N_i(t) = \sum_{k=1}^i \left\{ \left(\prod_{j=k}^{i-1} f_j \right) \cdot \left[N_k^0 \left(\sum_{j=1}^{i-k+1} d_j e^{-\lambda_j t} \right) + Y_k \left(\sum_{j=1}^{i-k+1} d_j \frac{1 - e^{-\lambda_j t}}{\lambda_i} \right) \right] \right\} \quad (2)$$

where:

$$d_j = \begin{cases} 1 & , (i = j = 1) \\ \frac{\prod_{k=1}^{i-1} \lambda_k}{\prod_{k=1}^i (\lambda_k - \lambda_j)} & , (i \geq 2, j \in [1, i]) \end{cases} \quad (3)$$

Incorporating the neutron reaction terms, one may observe that the transmutation rate $\sigma_{tr,k}\phi(t)$ behaves similarly to a decay constant in function and that the unit production rate per neutron reaction $g_{k\rightarrow i}$ behaves similarly to a decay branching ratio. With this in mind, at times with nonzero neutron flux, the decay constants λ_k and branching ratios $f_{k\rightarrow i}$ in Equations 2 and 3 can be replaced with the new effective decay constant λ_k^* and effective branching ratio $f_{k\rightarrow i}^*$, shown in Equations 4 and 5, respectively. This can be simply thought of as treating neutron reactions as an additional decay mode which only has a nonzero branching ratio while the primary source/beam is active.

$$\lambda_k^* = \lambda_k + \sigma_{tr,k}\phi(t) \quad (4)$$

$$f_{k\rightarrow i}^* = f_{k\rightarrow i} \frac{\lambda_k}{\lambda_k^*} + g_{k\rightarrow i} \frac{\sigma_{tr,k}\phi(t)}{\lambda_k^*} \quad (5)$$

Note that $\sigma_{tr,k}$ is the single-group average transmutation cross section given by Equation 6 with multi-group cross section $\sigma_{tr,k}^g$ and multi-group flux $\phi^g(t)$ at time t .

$$\sigma_{tr,k} = \frac{\sum_g \sigma_{tr,k}^g \cdot \phi^g(t)}{\sum_g \phi^g(t)} \quad (6)$$

These equations slightly differ in situations where a chain contains a nuclide whose decay constant is extremely close to that of another nuclide in the same chain or when the decay/reaction product of one nuclide in the chain is the same as another nuclide already appearing earlier in the chain (making a cyclic chain). A description of the handling of these cases and a more detailed derivation of all of these equations are provided in Reference 1. Additionally, a variety of checks and approximations are employed to handle extreme values while evaluating Equation 2, circumventing major numerical precision-induced errors.

Similar linear chain methodologies are also employed by other activation codes (e.g. CINDER [7]); though, differences are present, particularly with the handling of cyclic chains and near-equal decay constants. Alternative deterministic approaches for solving the system of Bateman differential equations utilized by other codes include the matrix exponential method (e.g. ORIGEN [8]) and numerical solvers (e.g. ALEPH-2 [19] which utilizes a Runge-Kutta method). Some codes include multiple methods such as Serpent [20] (linear chains and an advanced version of the matrix exponential method, CRAM [21]) and FLUKA [4] (a pure Monte Carlo “semi-analogue” approach and analytic solutions to the Bateman equations).

2.3. Usage of DCHAIN with PHITS

The intended usage of PHITS and DCHAIN together is illustrated in Figure 1; after a simulation scenario has been designed, the two codes are executed sequentially with no other intermediate action of the user required.

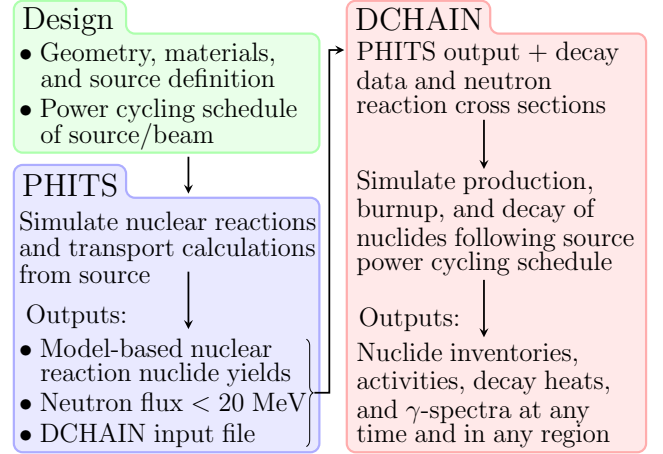


Figure 1: Flow of a coupled PHITS + DCHAIN simulation

As with any particle transport calculation, the geometry, materials, and source term must be defined first. In addition to this, the time-variation of the source’s power level must also be specified. For instance, one may state that an ion beam is on at 100% power for 2 hours, off for 30 minutes, and then on at 80% power for 3 hours. PHITS then handles all of the time-independent calculations of particle transport of the source through the geometry and any secondary reactions which may occur. Using the [T-Dchain] tally in PHITS, the neutron flux under 20 MeV, nuclide yields through higher-energy reactions (everything except for neutrons under 20 MeV), and an input file for DCHAIN are automatically generated. The time-dependent variance of the source’s power is simply passed along to DCHAIN here.

DCHAIN then takes over the time-dependent calculations. Using the source’s power schedule, DCHAIN determines what factors influence nuclide inventory at each time. Production and destruction through decay reactions are calculated at all times. While the source is on (above 0% power), it considers two additional nuclide production and destruction mechanisms: (1) low-energy neutron reactions and (2) high-energy reactions with all particles. The low-energy neutron calculations use the PHITS-calculated neutron flux spectra and DCHAIN’s internal transmutation cross section database(s). For the high-energy reactions, nuclide production and target burnup rates are determined by the PHITS-calculated nuclide yields.

DCHAIN outputs activity, decay heat, photon effective dose, and photon spectra in all regions of interest at any times requested by the user. This is all compiled into a primary output file, but useful supplementary files are also generated. For instance, the resulting decay photon spectra are outputted into file(s) formatted as PHITS source terms which can be directly reinserted into a secondary PHITS simulation, useful for determining dose distributions from residual radioactivity. Another, newly added, file illustrates the constructed nuclide production/decay chains and details how each chain contributes to nuclide

inventories with user-controlled granularity.

Understanding the internal methodologies and logic within DCHAIN is important for designing a simulation, obtaining consistent results, improving the calculation's efficiency (especially for more complex scenarios), and correctly interpreting the outputted information. Within a DCHAIN calculation, the simulation is divided into N_{reg} geometric regions specified by the user and $N_{\text{calc steps}}$ calculation time steps which are both specified by the user and automatically calculated in DCHAIN. This number of buildup and decay calculations performed in each region is a function of the times at which output is requested, the beam power cycling schedule, and the number of sub-steps $N_{\text{sub steps}}$ each irradiation time step is divided into (customizable, default of 50); this relationship is expressed in Equation 7 and is illustrated in an example in Figure 2.

$$N_{\text{calc steps}} = N_{\text{sub steps}} \cdot (N_{\text{irradiation}} + N_{\text{output, beam on}}) + N_{\text{cooling}} + N_{\text{output, beam off}} \quad (7)$$

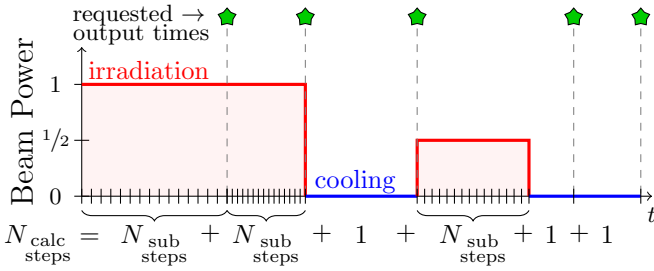


Figure 2: Determination of calculation steps from beam state and requested output times

Additionally, each calculation step's length (computational cost) T_{calc} is dependent on the complexity of the problem, as in the number of nuclides present and how they can decay, expressed in Equation 8 where $\delta_{\text{beam on/off}}$ is a delta function denoting whether the beam is on (1) or off (0) and N describes the quantity of what is specified by its subscript. During irradiation time steps, the calculation is considerably more complex since all of the neutron activation channels are opened as being possible, and the code explores all possible routes for decay and production of the present nuclides in each calculation time step.

$$T_{\text{calc}} \propto \sum_i^{N_{\text{nuclides present}}} N_{i, \text{decay pathways}} + \delta_{\text{beam on/off}} \cdot N_{i, \text{activation pathways}} \quad (8)$$

The variables in the earlier equations which vary with time, namely those dependent on $\phi(t)$ and $Y(t)$, are recalculated for all nuclides in each time step. While, for a given beam power, $Y(t)$ is usually nearly constant, DCHAIN does approximate the effect of high-energy nuclear reaction slowdown incurred from burnup of the target nuclides in these reactions. Then, in each time step in each region,

DCHAIN constructs all of the possible decay/reaction chains leading to the production of each nuclide present in the decay library database (by default limited to 100 unique chains per end-nuclide).

Then, calculating the change in inventory for each end-nuclide in a time step, DCHAIN sums the contributions of each chain which itself is the sum of all contributions from each nuclide in each chain as expressed earlier in Equation 2. Expressed more closely to how the calculation is actually handled by DCHAIN, the change in inventory ΔN of a single nuclide X_n in a single time step is shown in Equation 9 where C_{X_n} is the total number of chains/pathways leading to the production of nuclide X_n , L_ℓ is the length of (number of nuclides in) the ℓ^{th} chain, and $s_{\ell,m}$ is the m^{th} nuclide in the ℓ^{th} chain.

$$\begin{aligned} \Delta N_{X_n}^{\text{Total}} = & \Delta N_{\text{target} \rightarrow X_n}^{\text{model.reactions}} - \Delta N_{X_n \rightarrow *}^{\text{lib.reactions} + \text{decay}} \\ & + \sum_{\ell}^{C_{X_n}} \sum_{m}^{L_\ell} \left(\Delta N_{s_{\ell,m} \rightarrow X_n}^{\text{lib.reaction} + \text{decay(s)}} \right. \\ & \left. + \Delta N_{\text{target} \rightarrow s_{\ell,m} \rightarrow X_n}^{\text{model.reaction} \rightarrow \text{decay(s)}} \right) \end{aligned} \quad (9)$$

The first two terms of Equation 9 correspond to the two main terms of Equation 2 when $k = i$, and the summation terms describe $k < i$. In more detail, one can think of this as having two distinct portions: (1) production/destruction of X_n through direct reactions with X_n and (2) production of X_n through reactions of other nuclei.

This first direct portion is represented by the first two terms in Equation 9. $\Delta N_{\text{target} \rightarrow X_n}^{\text{model.reactions}}$ is direct production of X_n through beam/source interactions (everything but <20 MeV neutrons) from the PHITS-produced nuclide yield file which is reliant on physics model calculations; if X_n is a target nuclide, this term also includes model-calculated burnup of X_n . $-\Delta N_{X_n \rightarrow *}^{\text{lib.reactions} + \text{decay}}$ is loss of X_n through its decay and through neutron reactions transmuting it into something else (combined into a single term in DCHAIN), using the PHITS-produced neutron flux file and DCHAIN's neutron cross section library. DCHAIN includes these two terms in the final link of the first decay chain for each nuclide X_n and in none of the other subsequent chains for that nuclide.

The second portion of X_n produced through reactions of other nuclides is summed over all chains and all nuclides in each chain. In a similar fashion, this is split into two components for each nuclide in each chain. The $\Delta N_{s_{\ell,m} \rightarrow X_n}^{\text{lib.reaction} + \text{decay(s)}}$ term is the inventory of nuclide $s_{\ell,m}$ which was transmuted to X_n in that time step by decay(s) or neutron reaction possibly followed by decay(s), and $\Delta N_{\text{target} \rightarrow s_{\ell,m} \rightarrow X_n}^{\text{model.reaction} \rightarrow \text{decay(s)}}$ is the inventory of nuclide $s_{\ell,m}$ produced by beam/source (everything but <20 MeV neutrons) interactions with the region target material which subsequently underwent decay(s) to yield X_n .

3. Data library additions

For its calculations, DCHAIN employs both results calculated by PHITS as well as its own nuclear data libraries. DCHAIN relies on two primary types of nuclear data: neutron reaction cross sections and decay data. As already discussed, the cross section data is used for determining transmutation rates from the neutron flux. The decay data is used for constructing decay chains and calculating activities, decay heats, and photon spectra.

3.1. Decay data libraries

The decay library shipped with DCHAIN-SP prior to this work (alongside PHITS 3.13 and earlier) was largely the same as the original one from 1999, with some revisions and additions being made over time. This work introduces more modern evaluations from JENDL/DDF-2015 [22] and ENDF/B-VIII.0 [23], also with some specific data related to competing positron and electron capture decays from ENSDF [24]. Users may select between either of these two modern decay libraries, the original decay library, or between two hybrid combinations of the three. The first of these hybrid libraries uses data from JENDL/DDF-2015 where available, then pulls data from ENDF/B-VIII.0 for nuclides not present in the JENDL file, and finally pulls data from the original decay data file for the handful of nuclides exclusive to it; this is the default decay data library in DCHAIN. The second hybrid decay data library is constructed similarly but places priority on the ENDF data over the JENDL data. These decay libraries are summarized in Table 1.

Table 1: Decay data libraries in DCHAIN

Added in	Decay library source(s)	Ref.
1980	*Nuclear Data Sheets (1977)	[25]
1999	a combination of evaluations: EAF-3.1, FENDL/D-1, ENSDF (1997), Table of Isotopes 8 th ed. (1996), Chart of the Nuclides 1996	[26, 27] [28] [29] [30]
2019	JENDL/DDF-2015	[22]
2019	ENDF/B-VIII.0 (2018)	[23]
2019	combinations of the above	

*from the original DCHAIN, not present in DCHAIN-SP and newer

The 1999 decay library contained data for 3144 nuclides; this has been expanded to 4013 nuclides with the addition of the modern libraries. The majority of the new nuclides either lie on the fringes of the table of isotopes or are new isomeric states. However, the significant elements of the decay data for many previously included isotopes has changed notably. Figure 3 illustrates which isotopes had notable changes to their decay data between the new and old libraries. For the sake of this illustration, a nuclide’s data is considered “notably different” if at least one of the following three criteria is met:

1. Half-life changed by at least 10%. If changing to or from being listed as stable, this is only considered notable if the isotope’s radioactive listing had a half-life of 10^{14} seconds (3.17 million years) or shorter.
2. Average alpha, gamma, or beta emission energies changed by at least 10%, only considered notable if the changed value (E_α , E_γ , or E_β) represented at least 1% of the decay’s total energy released.
3. The primary decay mode/channel (the one with highest branching ratio) had changed.

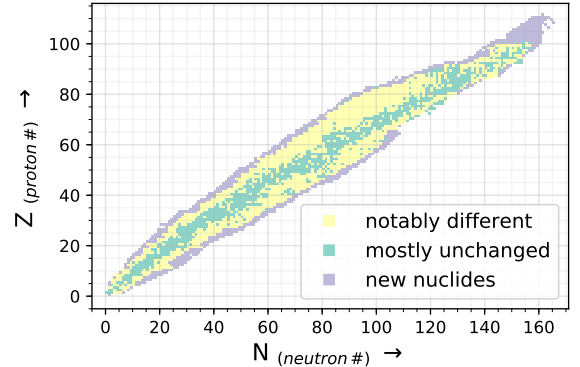


Figure 3: Nuclides newly added or whose decay data had a significant element changed by at least 10% between DCHAIN’s previous and current decay library

The majority of these “notable” differences stem from changes in average beta and gamma emission energies, implying the results most impacted by the updated decay libraries will be decay heat and photon dose/spectra.

DCHAIN utilizes three data files related to the decay data. The first is a comprehensive decay data file which is simply an extraction of the data needed by DCHAIN from the ENDF6-formatted¹ files and then translated into a DCHAIN-specific format. The second is a table containing photon fluence to effective dose coefficients for every nuclide in the decay library, and the third is a table specifying the positron emission fraction for nuclides undergoing competing positron emission and electron capture decays used in determining annihilation photon fluxes.

The photon fluence to effective dose file has been completely renovated in this update to DCHAIN. Users may now choose to use one of seven different conversion factors. The first six are photon fluence to effective dose E conversion coefficients published in ICRP 116 [31] for the various standard geometries: AP, antero-posterior; PA, postero-anterior; LLAT, left lateral; RLAT, right lateral; ROT, rotational; and ISO, isotropic. The seventh is fluence to ambient dose equivalent $H^*(10)$ conversion coefficients from

¹The ENDF acronym stands for both “Evaluated Nuclear Data File” and “Evaluated Nuclear Data Format.” To distinguish the two, the major version number of the “files” is written in Roman numerals while the “format” is versioned using Arabic numerals. Context also typically makes apparent whether the file or format is being discussed. Except for ENSDF, all nuclear data files discussed in this work utilize the ENDF format.

ICRP 74 [32] for photons 10 MeV and lower and from Pelliccioni [33] above 10 MeV.

To calculate the contribution of annihilation photons to the gamma-ray spectra and dose, it is important to know not only the total branching ratio of the positron emission (β^+) and electron capture (EC) decay channel but also the number of positrons emitted per unit decay through these two competing modes. However, within the ENDF-formatted decay databases and ENSDF, not all nuclides which undergo a positron emission or electron capture decay have the relative intensities of these competing decay modes clearly stated as the two channels are not split into separate decay modes in the ENDF format (see the MF=8 MT=457 entry of the ENDF6 manual [34]). Instead, it must typically be derived from the total average positron emission intensity per decay. However, this data in addition to the average annihilation photon yields per decay are not necessarily available either. In the case of DCHAIN's library assembled from JENDL/DDF-2015, ENDF/B-VIII.0, and ENSDF (from 2019), nearly 33% of all nuclides which have a listed β^+ /EC channel are missing this positron emission data.

Thus, to maintain the ability to accurately predict photon fluxes in DCHAIN when encountering a nuclide with such decay data deficiencies, an empirical model exists within DCHAIN to determine what fraction of decays emit a positron (subsequently creating annihilation photons) versus undergoing electron capture; this is referred to as the positron emission probability I_{β^+} . This work sought to improve this model.

Figure 4 shows the relationship between I_{β^+} , decay Q-value, and mass number A for a variety of β^+ /EC decays within JENDL/DDF-2015, ENDF/B-VIII.0, and ENSDF which have sufficient positron emission intensity information already available. The nearly horizontal blue line indicates the line below which all decays are exclusively 100% electron capture (0% positron emission); note that there are some 100% EC decays lying near but above this line. All points above the curved red line have a 99% positron emission probability or greater. Both of these lines were empirically generated.

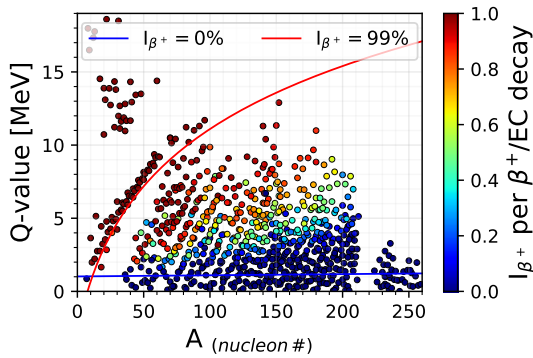


Figure 4: Relationship between known evaluated positron emission probabilities I_{β^+} , A, and Q

The empirical model for calculating the positron emission intensity I_{β^+} previously employed for this was a simple piece-wise function dependent on the decay's Q-value, Q_i , and the parent's mass number, A, using the functions listed in Equations 10 and 11.

$$Q_{th}(MeV) = 1.022 + (5 \times 10^{-3}) \cdot A \quad (10)$$

$$I_{\beta^+} = \begin{cases} 0.0 & Q_i < Q_{th} \\ \frac{Q_i}{2 \cdot Q_{th}} - \frac{1}{2} & Q_{th} < Q_i < 2 \cdot Q_{th} \\ \frac{Q_i - 2 \cdot Q_{th}}{10 - 2 \cdot Q_{th}} & Q_i > 2 \cdot Q_{th} \end{cases} \quad (11)$$

This work introduces a new empirical function that more accurately predicts the existing data. Provided Q and A should be the variables which impact I_{β^+} , one must note that the impact of Q on I_{β^+} is much more significant than that of A. Thus, the function decided on was a logistic function with Q as the primary variable (Equation 12), but the other coefficients within the main function have light dependencies on A (Equations 13 through 15). Since the change in I_{β^+} appeared more steep for decays of lower Q-values, a multiplier on the steepness of the logistic curve was adopted for decays of lower Q-value. The fitting parameters in these equations, denoted as c with subscripts, are tabulated in Table 2 and were optimized to minimize deviation with known values of I_{β^+} , first manually/visually and then refined using a generalized reduced gradient nonlinear solver [35].

$$I_{\beta^+} = \begin{cases} 0.0 & Q_i < Q_{th} \\ \left(1 + e^{-k \cdot (Q_i - Q_x)}\right)^{-1} & Q_i > Q_{th} \end{cases} \quad (12)$$

where:

$$Q_x = c_{x1} \cdot A^2 - c_{x2} \cdot A + c_{x3} \quad (13)$$

$$k = c_{k1} \cdot m \cdot A^{-c_{k2}} \quad \text{if } k > 5, \text{ then } k = 5 \quad (14)$$

$$m = \begin{cases} c_{m1} \cdot A + c_{m2} & Q_i < Q_x \\ 1.0 & Q_i > Q_x \end{cases} \quad (15)$$

Table 2: New I_{β^+} model parameters

Variable	Value
c_{x1}	10^{-4}
c_{x2}	2.14×10^{-4}
c_{x3}	2.2216
c_{k1}	168.18
c_{k2}	1.146
c_{m1}	2.94×10^{-3}
c_{m2}	2.818

Figure 5 illustrates the performance of the previous and new positron emission intensity estimation functions by overlaying a colormap of their equations over this phase space and the known $I_{\beta+}$ values shown earlier in Figure 4.

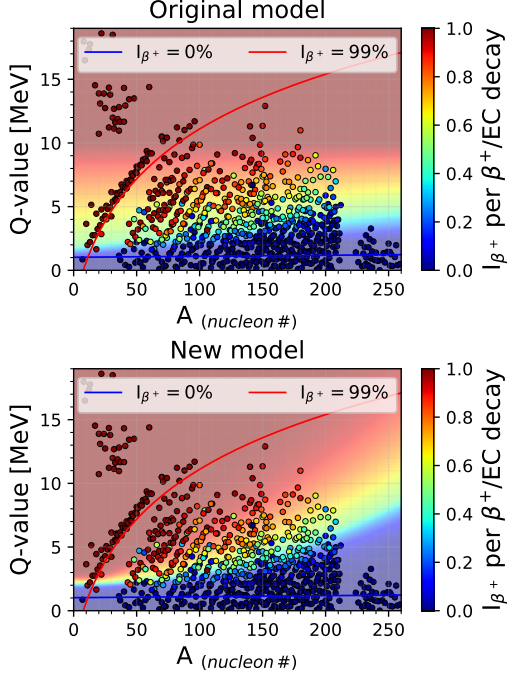


Figure 5: Known evaluated positron emission intensities per competing β^+ / EC decay with the (top) old and (bottom) new $I_{\beta+}$ estimation functions overlaid.

Through this exercise, the improvements of the new function relative to the original one are easily discerned. The previous function performs best for decays where electron capture is favored over positron emission. For heavier nuclides, where a larger fraction of the positron data is absent, it seems to overestimate $I_{\beta+}$ with Q-values above a few MeV, and it poorly estimates the heavily favored positron emissions from the lighter nuclides. The new model appears to fit the known data much more closely, and the boundaries where either decay mode becomes overwhelmingly more probable than the other also align well.

To quantify the improvement of this function, the differences between the known and calculated values are studied. Figure 6 shows the differences of known and calculated values from both models, and Table 3 summarizes their mean and median differences and R^2 values.

It is clear that systematic issues are present in the original model while deviations in the new model appear more random, though more concentrated at low-to-intermediate masses. While the mean and median differences from normal subtraction do not provide a conclusive judgment on which model performs best, the absolute differences of the known and calculated values make a much stronger case for the new model. Since calculated values can deviate above and below the known value, both models “on average” appear to perform well in predicting $I_{\beta+}$. However, when considering the absolute magnitude of the deviations, the

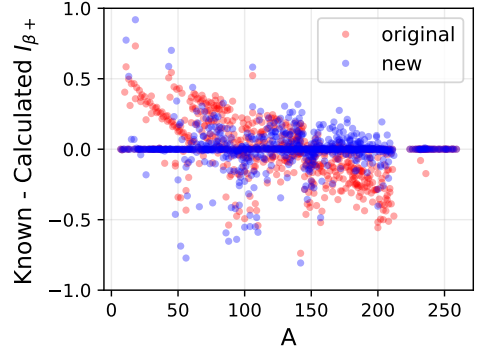


Figure 6: Differences between the known evaluated and calculated values are shown for both the new and old models predicting $I_{\beta+}$.

Table 3: Differences between known evaluated and calculated positron emission probabilities $I_{\beta+}$ (as percentages)

Quantity	Known - Calculated	
	Old model	New model
Mean	-0.73%	0.0011%
Median	0.00%	0.00%
*Mean _{abs}	12.39%	6.74%
*Median _{abs}	7.32%	1.27%
R^2	0.788	0.883

*calculated from the absolute value of the difference instead of the normal difference

issues from the systematic trends in the old model become much more evident; the R^2 value of each function against the evaluated data values affirms this. The new model more accurately estimates positron (and, thus, annihilation photon) emission rates without systematic over/under predictions dependent on the masses of activated nuclides.

3.2. Neutron reaction cross section libraries

Prior to this work, DCHAIN’s neutron reaction cross section library had undergone two major revisions, from the original 1980 27-group dataset (based on computer calculations [36] using 1976 JNDC [37] and BNL-325 [38] data) to the 175-group FENDL/A-2.0 library [13] (released in 1997) and then later to the 1968-group JEFF-3.1A library [14] (released in 2005). This work implemented a variety of modern neutron reaction cross section libraries from which the user can choose.

The DCHAIN library files were composed by converting the original point-wise ENDF-formatted cross section data files to group-wise ENDF format (in the 1968-group ECCO structure) with the PREPRO ENDF pre-processing code suite [39] and then extracting and compiling the information relevant to DCHAIN into a separate library data file with a dedicated Python script. Since these cross sections are used for assessing transmutation rates, elastic scattering and (n,n) reactions in general (except those resulting in a change of isomeric state) are of no interest to DCHAIN and are thus excluded. The available libraries and the number of unique nuclides and total transmuting reactions included within each are shown in Figure 7.

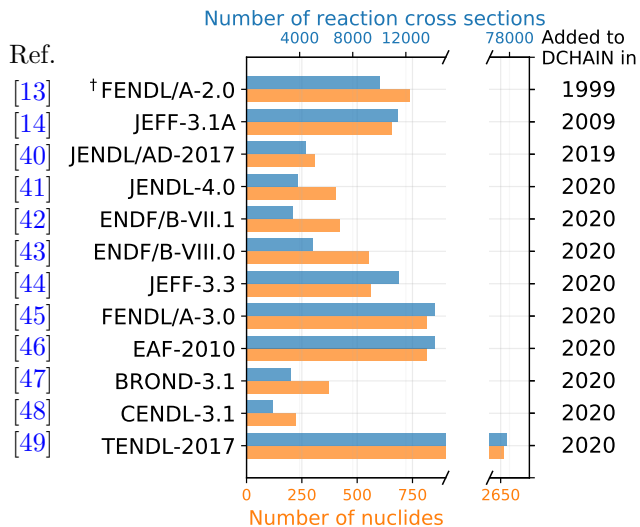


Figure 7: Neutron reaction cross section libraries in DCHAIN; †FENDL/A-2.0 is in the old 175-group structure, not the current default ECCO 1968-group structure.

As one may note, there is a large variance in expansiveness between the various libraries. TENDL, due to its model-based construction, has theoretical data for practically every reaction imaginable. In contrast, the more traditional, experimental data-focused evaluated databases such as JENDL and ENDF can appear lacking. The fusion-tailored libraries from Europe fit somewhere between these extremes, being largely based on evaluated experimental data but also supplemented with TALYS-calculated cross sections [50, 44, 45, 46].

When selecting a cross section library for a calculation, it is important to understand its origins, focus, and limitations. For instance, EAF, the European *Activation File*, is clearly built for activation calculations. JENDL/AD-2017, while also designed for activation calculations, is tailored to reactor decommissioning and only is concerned with nuclides with half-lives over 30 days [40]. The ENDF libraries, BROND, CENDL, and JENDL-4.0 are general purpose libraries which encompass many of the most typical reactions but are lacking some more niche reactions, particularly those involving isomers. Additionally, CENDL is missing isotopic cross sections for a number of elements, making derivation of specific transmutation cross sections from the reactions impossible.

To allow users to employ data from a preferred source but not feel as if they are compromising their results by not selecting one of the more expansive libraries, a handful of hybrid neutron reaction cross section libraries have been composed. Presently, these hybrid libraries are assembled from data taken from the Japanese (JENDL/AD-2017 and JENDL-4.0), American (ENDF/B-VIII.0), and European (JEFF-3.3 and FENDL/A-3.0) libraries. For instance, one library prioritizes selecting data from the Japanese, then American, and then European libraries. This library contains all of JENDL/AD-2017, reactions from JENDL-4.0 absent from JENDL/AD-2017, reactions from ENDF/B-

VIII.0 absent from either JENDL library, reactions from JEFF-3.3 absent from any of the JENDL or ENDF libraries, and finally any reactions within FENDL/A-3.0 not included already. This hybrid library is presently the default cross section library within DCHAIN. Users may also select from libraries prioritized as US→JP→EU or EU→US→JP as well as one library which is just a combination of both JENDL libraries.

When combining libraries in this fashion, one must take care not to double-count any reactions; this is of particular concern when isotopes with numerous isomeric states are involved. For instance, considering the (n,2n) reaction with ^{89}Y , whether the isomeric states of the product ^{88}Y are distinguished or not is dependent on the library. Within the ENDF and JEFF libraries, three separate (n,2n) reaction cross sections with ^{89}Y are provided, producing ^{88g}Y , ^{88m1}Y , and ^{88m2}Y . In the JENDL and FENDL libraries, only one cross section is provided for this reaction, and this single ^{88}Y production cross section is the sum of those for the three possible isomeric states. Naively, when composing a hybrid library prioritizing JENDL over ENDF, one may note that ENDF includes the two metastable state cross sections which JENDL does not and then opt to include those in addition to the “ground state” cross section provided by JENDL; though, this would be in error as then those two cross sections would be accounted for twice.

On a technical note, this availability stems from what sections are present in the ENDF-formatted files for each target nuclide. While all of them include MF 3 (“file 3”) sections for reactions cross sections, some also contain MF 10 sections specifically for radionuclide production cross sections where numerous cross sections for the isomeric states of the product nuclide can be provided. When the MF 10 section is present for a given reaction, there is no ambiguity on the identity of the product nuclides. When the MF 10 section is absent, only the element and atomic mass of the product can be obtained from either the MF 8 section (decay and fission product yields “file”) if present or derived from the reaction number MT; there is not a straightforward way of identifying the isomeric state of the product in those cases. Thus, when assembling these hybrid libraries, care was taken to avoid this double-counting error, only including either specific individual isomeric states of the product or all states combined for any given target and reaction.

4. New features and functionalities

In addition to the new decay and neutron reaction cross section data added to DCHAIN, a variety of new functionalities have also been implemented. This includes statistical uncertainty propagation, more detailed tracking of nuclide production, support for three-dimensional grid mesh and tetrahedral geometries, and efficiency and performance improvements. These features are expanded upon in the following subsections.

4.1. Statistical uncertainty propagation

DCHAIN-PHITS relies on two sets of values calculated by PHITS, neutron fluxes and nuclear reaction-induced nuclide yields, and both of these have statistical uncertainties associated with them due to the random nature of the Monte Carlo particle transport process. However, previous versions of DCHAIN did not include any uncertainty propagation, meaning one would need to be particularly careful in verifying that any results were statistically valid. With this update, these uncertainties are now propagated through the calculations to the final resulting inventories, activities, decay heats, photon doses, and photon spectra.

Referring to Equation 2, incorporation of the uncertainty in the PHITS-calculated nuclide yields $Y_k(t)$ is reasonably straightforward. The Y_k -dependent terms of the change in nuclide inventory ΔN_i are recalculated except substituting Y_k with its absolute uncertainty $\delta(Y_k)$ instead. Propagated through the rest of the calculation, this becomes the beam/high-energy reaction yield-attributable component of the uncertainty in ΔN_i .

Incorporating the uncertainty of the neutron flux is slightly more complex. The uncertain variable is the neutron flux $\phi(t)$, and it is used to calculate the single-group, flux-weighted transmutation cross sections $\sigma_{tr,k}$ which are then used to calculate the effective decay constants λ_k^* and effective branching ratios $f_{k \rightarrow i}^*$. The uncertainty of the product of this single-group cross section and the flux $\delta(\sigma_{tr,k} \cdot \phi(t))$ (the value actually used in calculating λ_k^* and $f_{k \rightarrow i}^*$) is calculated as shown in Equation 16 where $\delta(\phi^g(t))$ is the absolute uncertainty in the flux in energy bin g .

$$\delta(\sigma_{tr,k} \cdot \phi(t)) = \sqrt{\sum_{g=1}^{1968} [\sigma_{tr,k}^g \cdot \delta(\phi^g(t))]^2} \quad (16)$$

This uncertainty is then ultimately propagated through to the $f_{k \rightarrow i}^*$ terms of Equation 2 where the fractional uncertainty of the product of the $f_{k \rightarrow i}^*$ terms is calculated as the linear sum of the fractional uncertainties of each $f_{k \rightarrow i}^*$ term. The summation here is linear, rather than in quadrature, since the underlying neutron flux used to calculate each term is the same, making them no longer independent and random [51]. For instance, for a reaction chain involving two subsequent neutron capture reactions, it would be unfair to add their uncertainties in quadrature since the effective branching ratios of both were ultimately calculated from the same initial neutron spectrum. The yield and neutron flux uncertainties are then propagated using the conventional methodology of linear sums of absolute uncertainties (for sums and differences) and fractional uncertainties (for products and quotients) at each step until each nuclide inventory and its uncertainty are obtained.

4.2. Support for 3-D grid mesh and tetrahedral geometries

The geometry of a traditional PHITS simulation is constructed using simple surfaces (such as planes, spheres, cylinders, etc.) and cells/regions filling all space which are

constrained and defined by these surfaces, using Boolean logic. Tallies can then be built to count particles which either cross these surfaces or pass through these cells. Since DCHAIN seeks to determine nuclide inventories within a region, the [T-Dchain] tally fits in this latter category.

However, this style of geometry and tally definition is not always well-suited for every application. In cases where one may wish to study spatial distributions within a monolithic structure (such as what portions of a large wall are being activated), it is not convenient to define each tally region of interest individually. In these cases, PHITS provides the option to define a three-dimensional grid of tally volumes independent of the defined geometry, allowing for any resolution in grid size the user desires. While this functionality has been available in many PHITS tallies for some time, this update implements support for these types of tallies in DCHAIN as well. As a rather unique feature of DCHAIN, the grid voxels are not constrained to a single material. An individual voxel can contain region boundaries of different materials, and DCHAIN will properly account for the variety and respective volumes of each material in its calculations for that voxel. DCHAIN also now has the ability to automatically generate two-dimensional heatmap plots of the calculated activity along any of the three axes of these three-dimensional grid mesh tallies.

In other cases, particularly for more complex models, defining the geometry itself in the traditional way may be overly cumbersome. For that purpose, support for geometries defined as a collection of tetrahedrons, such as those which may be generated from geometries designed in a CAD software, was added first in PHITS 2.80 [52]. Over time, support for tetrahedral mesh geometries within PHITS has been expanded, allowing for increased efficiency for those working in interdisciplinary fields which are more likely to be utilizing these CAD geometries, such as fluid dynamics, thermal sciences, and nuclear medicine [53] in addition to more traditional nuclear scientists working with very complex geometries such as accelerator components and facilities. This update introduces support for these tetrahedrally defined geometries to DCHAIN. This unlocks some interesting possibilities for future simulations such as a thermal transport code utilizing time-dependent decay heats from DCHAIN. To more easily enable some of these studies, DCHAIN can also automatically produce files at any desired times containing the decay heat being produced in each tetrahedron formatted in a CSV and/or OpenFOAM [54] format for direct use with the ANSYS FLUENT [9] computational thermal and fluid dynamics code; output formatted for use with FLUENT is already supported in several other tallies within PHITS.

Both of these geometry types allow for substantially higher spatial resolution of activation results than what would be obtained from the more traditionally defined geometries. Additionally, these two geometry methods can be used together; one may utilize a tetrahedrally defined geometry in PHITS but overlay a 3-D grid mesh on it in the [T-Dchain] tally to obtain voxelized results.

4.3. Efficiency and performance improvements

While DCHAIN is generally significantly less computationally expensive and runs much faster than the precursory PHITS simulation, typically on the order of seconds (and, at most, minutes) for smaller geometries, the tetrahedral and 3-D grid mesh tallies which can contain vastly more individual regions than traditionally defined problems do have a significant impact on the run time of DCHAIN. At its core, DCHAIN treats all regions within a problem independently; for each, PHITS provides a specific neutron flux spectrum and set of nuclide yields, meaning production and destruction rates of nuclides are different in every region even if they contain the exact same initial material composition.

This work implements some performance improvements to mitigate this impact as much as possible. Now, by default, the neutron reaction cross section library is read and stored into system memory for the duration of a DCHAIN calculation rather than being reread for each region. Given the relatively large size of these libraries, particularly the modern ones which are on the order of 100 MB, one can understand the increased memory requirement but also the reduction of run time for not needing to read in a file of that size numerous times. Other performance and memory improvements have been implemented including (1) reformatting the PHITS output files containing the neutron flux spectra and nuclide yields for each region for improved space efficiency and (2) eliminating redundant file reading everywhere possible within DCHAIN, accelerating many-regioned calculations in particular in both PHITS and DCHAIN.

More concretely expressed, the total run time T_{total} of DCHAIN can be thought of as being composed of (1) time spent reading files—the decay data library $T_{\text{rd decay lib}}$, neutron cross section library $T_{\text{rd } \sigma \text{ lib}}$, neutron flux spectra $T_{\text{rd flux}}$, and nuclear reaction nuclide yields $T_{\text{rd yield}}$ —and (2) time spent actually constructing decay chains and performing calculations T_{calc} (Equation 8) in each of the $N_{\text{calc steps}}$ calculation steps (Equation 7) in each of the N_{reg} independent regions. The total calculation time utilizing the more efficient settings and data formats is shown in Equation 17; the T' variables denote files whose read times have been reduced by the new formatting. Before these efficiency improvements had been made to DCHAIN, this calculation time scaled as shown in Equation 18.

$$T_{\text{total}} \propto T_{\text{rd decay lib}} + T_{\text{rd } \sigma \text{ lib}} + T'_{\text{rd flux}} + T'_{\text{rd yield}} + \sum_{i=1}^{N_{\text{reg}}} \left(N_{\text{calc steps}} \cdot T_{\text{calc}} \right) \quad (17)$$

$$T_{\text{total}} \propto T_{\text{rd decay lib}} + \sum_{i=1}^{N_{\text{reg}}} \left(T_{\text{rd } \sigma \text{ lib}} + \frac{i}{N_{\text{reg}}} T_{\text{rd flux}} + T_{\text{rd yield}} + N_{\text{calc steps}} \cdot T_{\text{calc}} \right) \quad (18)$$

Understanding these relationships impacting run time can be quite important, especially if needing to run many DCHAIN simulations or ones composed of many regions. Recalling that DCHAIN's calculation time is dominated by irradiation time steps due to increased complexity in available reaction pathways and subdivision into smaller steps, one can significantly impact the computational cost of a calculation through design of the irradiation schedule and requested output times.

4.4. New decay chain scheme file

A new output file has been added to DCHAIN in this work. While the default primary output file of DCHAIN provides detailed information on the inventories and other relevant quantities derived from it at the times requested by the user, it provides no information on specifically how each nuclide is produced. In short, this new output file allows the user to track what decay chains and reactions are responsible for the production of each nuclide with a variable amount of granularity. At its most detailed, the contribution from every reaction in every decay chain for every end-nuclide can be tracked at every time step calculated within DCHAIN.

As discussed earlier, DCHAIN splits a problem into independent calculations within each region. The user provides an irradiation schedule and times at which output is requested. DCHAIN then determines the number of discrete time steps over which calculations will be performed. This is initially single steps between each unique time inputted by the user where either the source's power changes or output is requested; time steps which take place while the source's power is nonzero are then further subdivided into $N_{\text{sub steps}}$ smaller time steps (50 by default). In the primary output file, only time steps in which output are requested are printed. In this new output file, the user can view inventories at every one of these $N_{\text{calc steps}}$ discrete time steps used within DCHAIN, if desired.

For each resulting end-nuclide, DCHAIN constructs up to, by default, 100 potential “decay” chains leading to its production, recalling that while the source/beam is “on” (power > 0) that neutron reactions are included as “decay” pathways within these chains. This new output file provides plaintext decay schemes for each of these decay chains resulting in the production of each end-nuclide. Furthermore, the contribution of each link within each decay chain to the change in inventory of the end-nuclide within a time step can also be printed, and this contribution is further sub-divided into the portion from high-energy reactions from the source and the portion from neutron reactions and/or decays (the terms from Equation 9). This allows for one to track specifically which reactions are most responsible for the production of each nuclide.

Since this is a rather high, sometimes excessive, level of detail possible, the user may adjust the granularity of the presented results through extra input options. This output file provides a much more detailed look at the inner workings of DCHAIN than was previously available.

It also allows for DCHAIN to be a far more useful tool for some specific applications such as designing low activation materials or target design for production of specific radioisotopes since it details exactly which reactions are contributing to the inventories of the nuclides of interest.

5. Results and discussion

This section seeks to demonstrate some of these new capabilities of and additions to DCHAIN through several example calculation scenarios.

5.1. Activity distribution within a copper beam dump

Understanding the activation products within an ion accelerator's beam dump is imperative for radiation protection during operation and decommissioning, and beam dumps could also serve as valuable sources of particular exotic isotopes with no other viable production pathways [55]. Due to its desirably high thermal conductivity, copper is commonly selected as a core material for accelerator beam dumps and is the material studied here. The radionuclide inventory of one such copper beam dump from the 1.8 mA 590 MeV proton accelerator at the Paul Scherrer Institute was experimentally analyzed in Schumann et al. [55]; this example calculation emulates it.

The study states that the beam dump had been in service for ten years and had been left to cool for one year before measurements were made; though, neither the duty cycle of the accelerator nor the beam radius had been detailed. For the sake of simplicity, it was assumed that the beam was pencil-like with a radius of $5\text{ }\mu\text{m}$ and operated at 10% power continuously for the 10-year period followed by a year of cooling. The beam dump, slightly simplified, is effectively a copper cylinder with radius 4 cm and length 30 cm and is composed almost entirely of copper with a variety of impurities, of which iron is the most abundant (60 ppm by weight) [55]. In this example, five million event histories (source protons) were simulated in PHITS, and then DCHAIN was used to determine the time-dependent inventories of all nuclides. A wide variety of nuclides are produced, but the activities of two of the most radiological significant, ^{60}Co and ^{55}Fe , are mapped as a function of position within the copper rod in Figure 8 along with their fractional uncertainties. These activities seem generally sensible; however, one may note the anomalies occurring at the axial positions near the end of the beam dump.

The activity spatial distributions should be continuous, and it appears as such in the areas of high statistical fidelity. Approaching the end of the beam dump where specific nuclide yield uncertainties begin to become poor, fluctuations in the spatial distribution of activity become more apparent. In the two anomalous regions of the ^{55}Fe distribution, one may note that the relative error in these regions is actually near zero despite neighboring regions having high uncertainties. Both of these nuclides are predominantly produced through high-energy nuclear reactions with the beam, but both, particularly ^{60}Co , also have

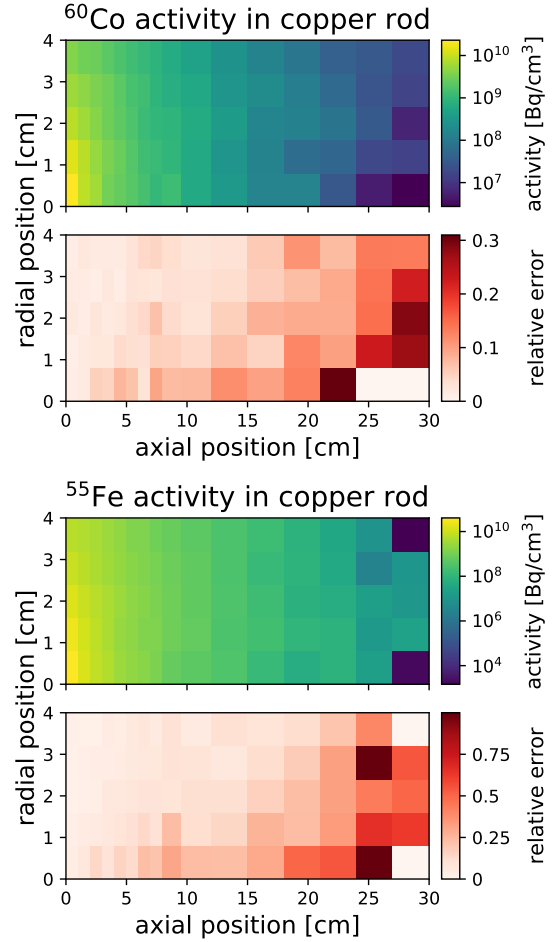


Figure 8: Spatial distributions of ^{60}Co (top) and ^{55}Fe (bottom) activity and relative error in the copper beam dump.

a small amount produced through low-energy neutron reactions.

Since the neutron fluxes generally have much lower uncertainties than yields of specific nuclides, in cases where no direct nuclear reactions producing the nuclide of interest are encountered in the PHITS simulation in that region, the amount of that nuclide produced and its uncertainty are solely based on the neutron flux. This is what is occurring in the anomalous regions of Figure 8. Using the newly added decay scheme file discussed earlier, the production mechanisms at play and their relative contributions to nuclide inventories can be directly verified. Throughout the whole beam dump, 85.7% of the ^{60}Co is produced through high-energy beam and secondary reactions with the remaining 14.3% produced through the $^{63}\text{Cu}(n,\alpha)^{60}\text{Co}$ reaction channel from secondary neutrons at or below 20 MeV. For ^{55}Fe , 94.716% is produced directly through beam reactions, 5.278% is through decay of ^{55}Co (which itself is produced almost entirely, >99.9999%, directly through beam reactions), and the remaining 0.006% is produced primarily through $^{56}\text{Fe}(n,2n)^{55}\text{Fe}$ reactions and a trace amount of the $^{58}\text{Ni}(n,\alpha)^{55}\text{Fe}$, $^{54}\text{Fe}(n,\gamma)^{55}\text{Fe}$, and $^{56}\text{Co}(n,np)^{55}\text{Fe}$ reactions.

The relative prominence of production from low-energy secondary neutron reactions versus direct beam and high-energy reactions increases as one moves further from the front surface of the beam dump. Due to this and the neutron reaction production channel being significant for ^{60}Co , the activity map remains smooth at the end of the dump while the uncertainty map is not. Since secondary neutron reaction production of ^{55}Fe is far less significant, the regions where no direct beam production of it was simulated (due to Monte Carlo statistical fluctuations and running the simulation for a finite amount of time) contrast starkly with neighboring regions where some, if only a few, ^{55}Fe -producing beam/secondary reactions took place. Thus, while also a generally important piece of information for any following calculations or assessments, the uncertainty data also can assist in troubleshooting any odd results and assist in determining if a PHITS simulation should be ran for longer or employ variance reduction techniques to improve statistics.

5.2. Carbon ion therapy-induced activity in a patient

Support for tetrahedral mesh geometries opens a new realm of complex problems possible for DCHAIN to tackle. As mentioned earlier, codes wishing to couple decay heat terms to heat/fluid transport problems may now do so using DCHAIN. This example, however, seeks to explore a different class of problems now available: spatial distributions of activation in more complex geometries.

Here, secondary activation of a patient by carbon ion therapy is quantified. In this example, the subject is irradiated by a 10^9 ion/second 150 MeV/n carbon ion beam of radius 1 cm for one hour (a feasible treatment at a variety of facilities such as HIMAC in Japan [56]). The patient is a lower-resolution version of the widely-used Stanford Bunny [57] 3-D test model which, after some additional processing with TetGen [58], is composed of 3875 tetrahedrons and has been scaled up to be approximately the size of a real rabbit; the model used could be tightly circumscribed by a box of dimensions 30 cm \times 30 cm \times 24 cm. The patient is simulated as being composed entirely of ICRP soft tissue (predominately hydrogen, carbon, and oxygen with small amounts of nitrogen and other elements) as described in the NIST STAR database [59]. The distribution of volume-normalized total activity in each tetrahedron immediately after the end of this irradiation period is depicted in Figure 9².

The area of highest activation coincides with the region leading up to the range of the carbon beam in soft tissue, about 5.5 cm, where the majority of the beam's energy is deposited. The exterior is notably less activated than the interior in the area around the beam trajectory, and the most prominent nuclides contributing to activity

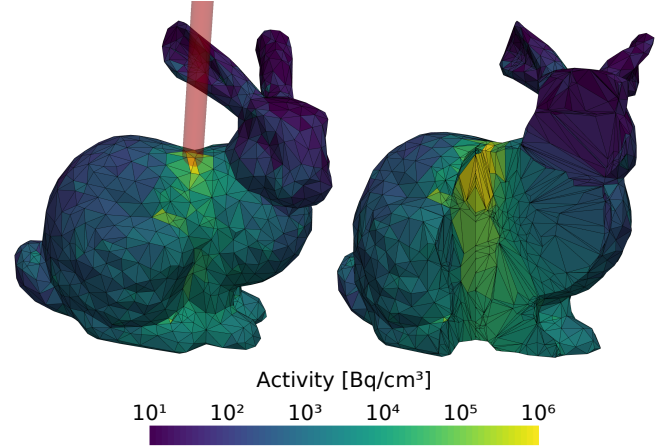


Figure 9: Volume-normalized activity in each tetrahedron immediately after end of irradiation. The left image shows the whole exterior of the bunny with the beam trajectory superimposed in red, and the right image has a 90° wedge removed to better illustrate the internal activity distribution.

at this time are ^{11}C , ^{16}N , and ^{15}O . Noting the logarithmic color scale, one can see that the activation is quite localized around the target area, diminishing several orders of magnitude when moving away and toward the head.

While this example serves just to demonstrate the new capabilities of DCHAIN, one can easily see the utility this specific type of simulation could serve if using a more realistic human phantom model with proper organs and their respective materials. Patient activation was not traditionally of concern with older photon-based treatments, but it is becoming increasingly relevant as high-energy ion treatments gain prominence since their spallation products and reactions from secondary neutrons result in notable activation [61].

This also serves as an opportunity to showcase the impact of the performance improvements implemented with the recent updates to DCHAIN. In the simulations leading to the results shown in Figure 9, the PHITS simulation calculated 25 million initial particle histories (broken down into 25 batches of one million), and the following DCHAIN calculation subdivided the one-hour irradiation period into fifty calculation time substeps. All calculations were performed on one CPU core with no multi-threading. Utilizing the more efficient file formats for the files generated by PHITS and the other performance/efficiency improvements in DCHAIN, the PHITS simulation took 47.8 hours to complete, and the subsequent DCHAIN calculation required 1.7 hours (101 minutes). To quantify the significance of the performance improvements, this whole process was repeated but using the old file formats and with the DCHAIN performance improvements toggled off, assuming its previous default behavior. In this case, the PHITS simulation took 49.0 hours to complete, and the DCHAIN calculation took 4.1 hours (249 minutes). Also worth consideration, the neutron flux and nuclide yield files generated by PHITS together totaled 100 MB with

²These renderings were generated using the PyVista Python library [60] from VTK-formatted files assembled separately using the tetrahedral mesh geometry input files used by PHITS and the CSV-formatted results produced by DCHAIN.

the new format while occupying 391 MB when using the older format.

In this particular case, PHITS spent the vast majority of its time performing particle transport calculations for the carbon beam and its secondary particles. The burden of writing these output files is only felt significantly for problems with many regions and especially so when the selected source term is faster to transport (such as less energetic protons). Still, the most significant improvement noted here is with the performance of DCHAIN, in this case taking less than half the time when using the efficiency improvements. While not an issue for DCHAIN since every region is treated independently, physical memory (RAM) usage with PHITS scales with the number of regions and tallies, and this can be a performance bottleneck for complex problems being ran on machines with low memory if accessing virtual memory is necessitated. One should also note again that the DCHAIN run time scales directly with the number of regions present; thus, for relatively simple calculations with a small number of regions rather than the nearly 4000 here, DCHAIN typically runs in seconds to, at most, minutes.

5.3. Secondary photon dose from activated target and room

Dose evaluations from activated materials using the DCHAIN-calculated photon spectra as the input source term for a secondary PHITS calculation are now one of the most powerful applications of DCHAIN. While DCHAIN can output PHITS-formatted photon source terms for each region regardless of geometry type, when used with 3-D grid mesh problems the resulting photon source card can now be directly inserted into a PHITS input file with no extra modification required from the user.

In this example, a brass cube of edge length 40 cm is bombarded with a 1 mA 500 MeV proton beam (range ≈ 20.5 cm) for 5 hours and left to cool for 15 minutes. The cube is placed 110 cm above the floor, and the room is three meters tall with 50 cm thick concrete walls, floor, and ceiling, illustrated in Figure 10a. After running this PHITS simulation and the automatically generated input file through DCHAIN, the activation profile depicted in Figure 10b is obtained; this is simply the sum of all activity in each voxel of a slice of the room including the target and 50 cm above and below it. Then, the resulting photon source spectra from the activated target and concrete are inserted back into the original PHITS input file, replacing the proton source, and simulated to produce the photon effective dose rate map shown in Figure 10c; this uses ICRP 116 fluence to dose conversion factors and is tallying all particles in the first two meters of air above the floor.

Since DCHAIN can yield the time-dependent spatially-distributed photon source term, PHITS and DCHAIN can be used together for a variety of activation and shielding applications to determine appropriate cooling periods and shielding configurations in addition to informing more fundamental design decisions like optimizing material choices

to minimize activation. For instance, if one were to introduce a 10 cm thick 304 stainless steel door leading from the corridor into the irradiation room and two 5 cm thick and 2 m tall stainless steel shields placed perpendicularly to each other next to the target after the end of the irradiation period, the photon effective dose rates throughout the room could be reduced as shown in Figure 10d.

Studying Figure 10d in contrast to Figure 10c, one can see that the shielding is reasonably effective but also that the activated concrete walls, especially near the entrance of the corridor, are a significant contributor to the effective dose rate. Iterating on this example, Figure 11 shows the room's photon effective dose rate as a function of cooling time after irradiation. By simply waiting a few hours, the effective dose rate in the main portion of the room is halved while allowing the target and room to cool for 12 hours allows for an order-of-magnitude reduction.

The plots in Figures 10 and 11 were created directly by PHITS and DCHAIN automatically (with minor formatting adjustments) using the included and coupled postscript-powered ANGEL plotting code.

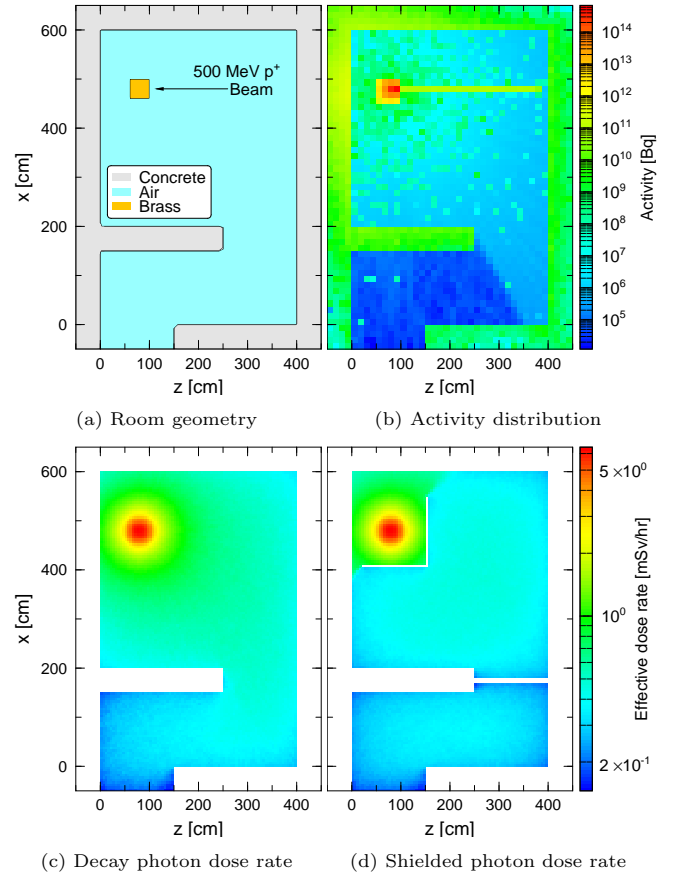


Figure 10: The room geometry in (a) underwent the specified irradiation in PHITS, activating the room elements as shown in (b) in DCHAIN, and the resulting photon effective dose rate distribution in air simulated in PHITS is shown in (c) with shielding added in (d).

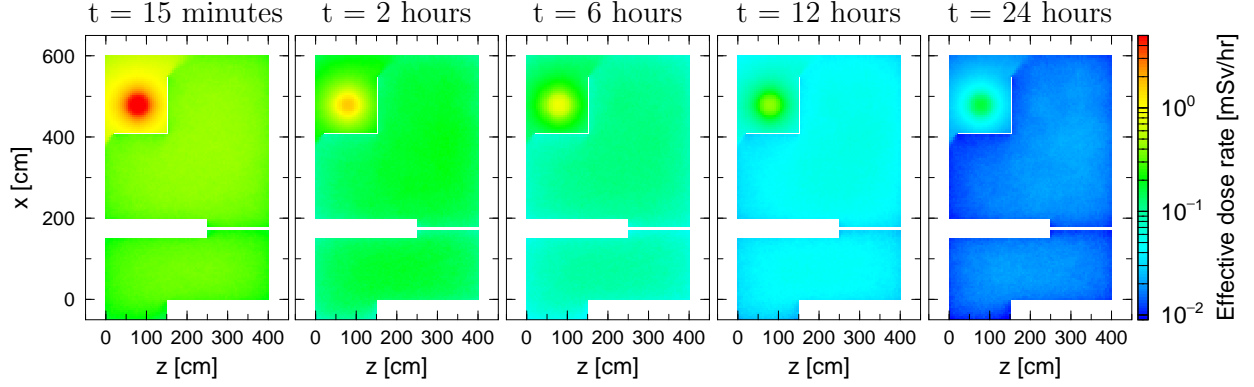


Figure 11: Decay photon effective dose rate with stainless steel shielding in place as a function of cooling time

5.4. Production of ^{177}Lu in a high flux reactor

With the addition of a variety of modern nuclear data libraries, DCHAIN can now also be used as a tool for comparing them. This example calculation studies production of the medical isotope ^{177}Lu as a function of irradiation time in a high flux reactor environment, in this case the Belgian Reactor 2 (BR2) with an assumed steady total neutron flux of $10^{15} \text{ n}/(\text{cm}^2 \cdot \text{sec})$, via irradiation of a 99.72% ^{176}Yb enriched (natural abundance of 12.76%) Yb_2O_3 target. This relies on a neutron capture reaction of ^{176}Yb to form ^{177}Yb which β^- decays with a 1.9 hour half-life to ^{177}Lu . The results of this simulation are shown in Figure 12 for several different neutron reaction cross section libraries used in DCHAIN.

While the results are in reasonable agreement, the differences in yield of ^{177}Lu depending on which neutron reaction cross section library is used could have significant financial/supply consequences since the ENDF-predicted yields (for which JENDL and BROND are in agreement with) are 7% higher than the JEFF-3.3-predicted yields

which are, in turn, 4% higher than the FENDL/A-3.0-predicted yields (for which JEFF-3.1A and EAF-2010 are in agreement with) at $t=10$ days. At $t=30$ days (after the most probable extraction time), those two percentages become 11.6% and 8.8%, respectively.

If this calculation is performed again but using the “direct” method of production instead—irradiating a target of enriched ^{176}Lu to produce ^{177}Lu through a single (n, γ) reaction—use of the different libraries results in similar discrepancies. Given this method’s importance in its substantially higher yields (but lower specific activities due to the chemically inseparable other isotopes of lutetium present), these data library differences illustrate a need for more measurements to be made of the ^{176}Yb and ^{176}Lu neutron absorption cross sections and/or for the existing evaluated data libraries to have their evaluations of these cross sections reassessed. Figure 13 shows these two cross sections relevant to ^{177}Lu production for the featured libraries. The extent and character of the resolved resonance region as well as the behavior beyond about 100 keV differs notably between the libraries.

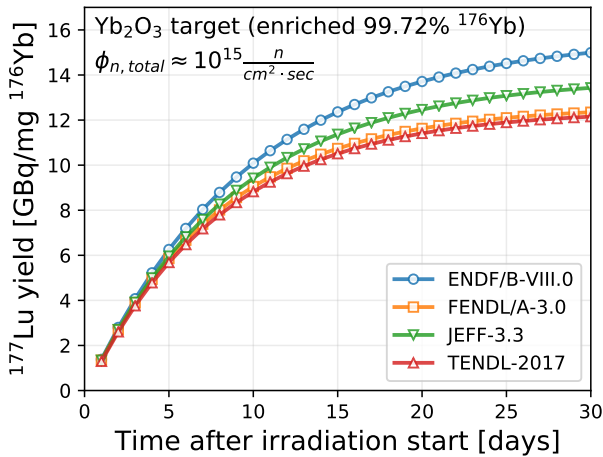


Figure 12: Yield of ^{177}Lu per unit mass of ^{176}Yb in the target as a function of irradiation time from bombardment of a Yb_2O_3 target (enriched to 99.72% ^{176}Yb) in a $10^{15} \text{ n}/(\text{cm}^2 \cdot \text{sec})$ neutron flux of similar profile to that of BR2 [62].

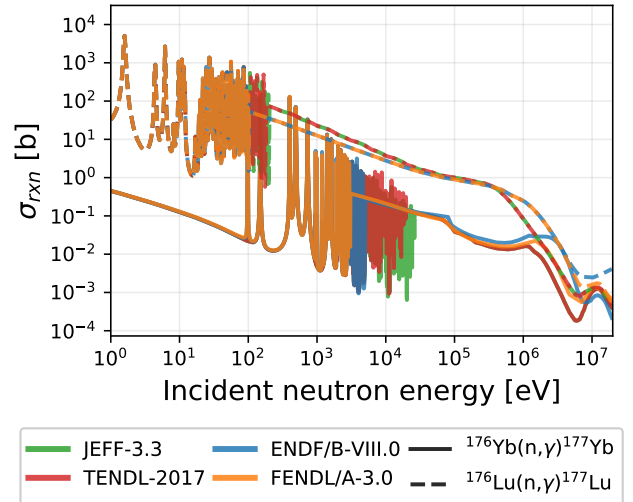


Figure 13: (n, γ) reaction cross sections for ^{176}Yb and ^{176}Lu

6. Conclusions

These recent efforts have sought to modernize DCHAIN and extend its coupling to the PHITS code. With the implementation of statistical uncertainty propagation and support of additional geometric configurations, DCHAIN-PHITS operates and produces output much more consistent with PHITS than before. The addition of new modern decay and neutron reaction cross section libraries allow for users both to select a preferred data source and to perform comparative calculations between the libraries. With the newly added decay chain scheme output file, users can obtain a much more detailed glimpse at the inner workings of a DCHAIN calculation, track every transmutation influencing the change in inventories of nuclides, and far more easily determine specifically what decays/reactions are most significantly impacting the inventories of nuclides of interest.

The newly introduced support for tetrahedral meshes unlocks usage of DCHAIN with complex CAD-generated geometries and more streamlined coupling to other scientific analysis tools such as FLUENT, and the additional features implemented for 3-D grid meshes allow for automatic visualization of DCHAIN results and easy transfer of the resulting decay photon spectra directly into a secondary PHITS simulation to then tally photon dose. The performance improvements made to DCHAIN provide substantial run time reductions for these large simulations too.

Overall, these improvements to DCHAIN successfully bring the code's capabilities into line with modern expectations, providing more flexibility regarding input and more variety in options for calculation parameters and output control. The most recent version of PHITS, which includes DCHAIN-PHITS, is freely available and can be obtained by applying at the official PHITS website <https://phits.jaea.go.jp/>.

CRedit authorship contribution statement

Hunter N. Ratliff: Writing - Original Draft, Conceptualization, Methodology, Software, Formal analysis, Visualization. **Norihiro Matsuda:** Conceptualization, Methodology, Software. **Shin-ichiro Abe:** Software, Supervision. **Takamitsu Miura:** Software. **Takuya Furuta:** Software. **Yosuke Iwamoto:** Software. **Tatsuhiko Sato:** Supervision, Writing - Review & Editing.

Acknowledgments

The author would like to thank Tetsuya Kai, Chikara Konno, and Kensaku Sakamoto from the Japan Atomic Energy Agency for sharing their advice and expertise early in this work.

References

- [1] K. Tasaka, DCHAIN 2: a computer code for calculation of transmutation of nuclides, Tech. Rep. JAERI-M 8727, Japan Atomic Energy Research Inst. (1980). doi:10.11484/jaeri-m-8727.
- [2] T. Kai, F. Maekawa, Y. Kasugai, H. Takada, Y. Ikeda, K. Kosako, DCHAIN-SP 2001: High energy particle induced radioactivity calculation code (2001). URL http://inis.iaea.org/search/search.aspx?orig_q=RN:32045280
- [3] T. Sato, Y. Iwamoto, S. Hashimoto, T. Ogawa, T. Furuta, S. ichiro Abe, T. Kai, P.-E. Tsai, N. Matsuda, H. Iwase, N. Shigyo, L. Sihver, K. Niita, Features of Particle and Heavy Ion Transport code System (PHITS) version 3.02, Journal of Nuclear Science and Technology 55 (6) (2018) 684–690. doi:10.1080/00223131.2017.1419890.
- [4] T. T. Böhlen, F. Cerutti, M. P. W. Chin, A. Fassò, A. Ferrari, P. G. Ortega, A. Mairani, P. R. Sala, G. Smirnov, V. Vlachoudis, The FLUKA Code: Developments and Challenges for High Energy and Medical Applications, Nuclear Data Sheets 120 (2014) 211 – 214. doi:<https://doi.org/10.1016/j.nds.2014.07.049>. URL <http://www.sciencedirect.com/science/article/pii/S0090375214005018>
- [5] F. Gallmeier, Activation calculations in accelerator environments an overview, in: Shielding aspects of accelerators, targets and irradiation facilities-Satif-10, 2010.
- [6] D. B. Pelowitz, MCNPX USER'S MANUAL Version 2.7.0 LA-CP-11-00438, Los Alamos National Laboratory (2011).
- [7] W. B. Wilson, S. T. Cowell, T. R. England, A. C. Hayes, P. Moller, A manual for CINDER'90 version 07.4 codes and data, Los Alamos National Laboratory, LA-UR-07-8412 (2008).
- [8] M. J. Bell, ORIGEN: the ORNL isotope generation and depletion code, Tech. rep., Oak Ridge National Lab., Tenn.(USA) (1973).
- [9] A. Fluent, et al., 12.0 User's guide, Ansys Inc 6 (2009).
- [10] K. Tasaka, DCHAIN: Code for Analysis of Build-up and Decay of Nuclides, Tech. Rep. JAERI 1250, Japan Atomic Energy Research Inst. (1977). doi:10.11484/jaeri-1250.
- [11] H. Takada, K. Kosako, Development of the DCHAIN-SP code for analyzing decay and build-up characteristics of spallation products (1999). URL https://inis.iaea.org/search/search.aspx?orig_q=RN:30031678
- [12] T. Kai, F. Maekawa, Y. Kasugai, H. Takada, Y. Ikeda, K. Kosako, Reliability assessment of high energy particle induced radioactivity calculation code DCHAIN-SP 2001 by analysis of integral activation experiments with 14 MeV neutrons, Tech. Rep. JAERI-Research 2002-005, Japan Atomic Energy Research Inst. (2002). doi:10.11484/jaeri-research-2002-005.
- [13] A. B. Pashchenko, H. Wienke, J. Kopecky, J. C. Sublet, R. A. Forrest, FENDL/A-2.0 Neutron activation cross section data library for fusion applications, Tech. Rep. IAEA-NDS-173(rev0), International Atomic Energy Agency (IAEA) (1997).
- [14] A. Koning, R. Forrest, M. Kellett, R. Mills, H. Henriksson, Y. Rugama, O. Bersillon, O. Bouland, A. Courcelle, M. C. Duijvestijn, et al., The JEFF-3.1 nuclear data library-JEFF report 21, Tech. rep., Organisation for Economic Co-operation and Development (2006).
- [15] E. Sartori, VITAMIN-J, a 175 group neutron cross section library based on JEF-1 for shielding benchmark calculations, JEF/DOC-100 (1985).
- [16] G. Rimpault, Physics documentation of ERANOS: the ECCO cell code, CEA Technical Note RT-SPRC-LEPh-97-001 (1997).
- [17] H. Takada, M. Harada, K. Kosako, Improvement of activation cross section library for high energy particle induced radioactivity calculation code DCHAIN-SP 2001, in: Atomic Energy Society of Japan 2009 Fall Meeting, J-PARC Material and Life Science Experimental Facility, 2009. URL <https://jopss.jaea.go.jp/search/servlet/search?5020767&language=1>

- [18] H. Bateman, The solution of a system of differential equations occurring in the theory of radio-active transformations, *Proc. Cambridge Phil. Soc.*, 1908 15 (1908-1910) 423–427.
- [19] A. Stankovskiy, G. Van den Eynde, Advanced Method for Calculations of Core Burn-Up, Activation of Structural Materials, and Spallation Products Accumulation in Accelerator-Driven Systems, *Science & Technology of Nuclear Installations* (2012).
- [20] J. Leppänen, M. Pusa, T. Viitanen, V. Valtavirta, T. Kaltiaisenaho, *The Serpent Monte Carlo code: status, development and applications in 2013*, *Annals of Nuclear Energy* 82 (2015) 142 – 150, joint International Conference on Supercomputing in Nuclear Applications and Monte Carlo 2013, SNA + MC 2013. Pluri- and Trans-disciplinarity, Towards New Modeling and Numerical Simulation Paradigms. doi:<https://doi.org/10.1016/j.anucene.2014.08.024>. URL <http://www.sciencedirect.com/science/article/pii/S0306454914004095>
- [21] M. Pusa, *Numerical methods for nuclear fuel burnup calculations* (2013). URL <http://urn.fi/URN:ISBN:978-951-38-8000-2>
- [22] J. Katakura, F. Minato, *JENDL Decay Data File 2015*, no. JAEA-Data/Code 2015-030, 2016. URL <https://www.ndc.jaea.go.jp/ftpnd/jendl/jendl-ddf-2015.html>
- [23] D. A. Brown, M. B. Chadwick, R. Capote, A. C. Kahler, A. Trkov, M. W. Herman, A. A. Sonzogni, Y. Danon, A. D. Carlson, M. Dunn, D. L. Smith, G. M. Hale, G. Arbanas, R. Arcilla, C. R. Bates, B. Beck, B. Becker, F. Brown, R. J. Casperson, J. Conlin, D. E. Cullen, M.-A. Descalle, R. Firestone, T. Gaines, K. H. Guber, A. I. Hawari, J. Holmes, T. D. Johnson, T. Kawano, B. C. Kiedrowski, A. J. Koning, S. Kopecky, L. Leal, J. P. Lestone, C. Lubitz, J. I. M. Damián, C. M. Mattoon, E. A. McCutchan, S. Mughabghab, P. Navratil, D. Neudecker, G. P. A. Nobre, G. Noguere, M. Paris, M. T. Pigni, A. J. Plompen, B. Pritychenko, V. G. Pronyaev, D. Roubtsov, D. Rochman, P. Romano, P. Schillebeeckx, S. Simakov, M. Sin, I. Sirakov, B. Sleaford, V. Sobes, E. S. Soukhovitskii, I. Stetcu, P. Talou, I. Thompson, S. van der Marck, L. Welter-Sherill, D. Wiarda, M. White, J. L. Wormald, R. Q. Wright, M. Zerkle, G. Žerovnik, Y. Zhu, *ENDF/B-VIII.0: The 8th major release of the nuclear reaction data library with CIELO-project cross sections, new standards and thermal scattering data*, *Nuclear Data Sheets* 148 (2018) 1 – 142, special Issue on Nuclear Reaction Data. doi:<https://doi.org/10.1016/j.nds.2018.02.001>. URL <https://www.sciencedirect.com/science/article/pii/S0090375218300206>
- [24] From ENSDF database as of January 1, 2019. Version available at <http://www.nndc.bnl.gov/ensarchivals/>.
- [25] W. B. Ewbank, F. E. Bertrand, *Nuclear data sheets*, *Nuclear Data Sheets* 20 (4) (1977) 429–549.
- [26] J. Kopecky, D. Nierop, *Contents of EAF-3*, Tech. rep., Netherlands Energy Research Foundation (ECN) (1992).
- [27] A. Pashchenko, Status of FENDL activation file and plans for the future developments, in: *Proc. Int. Workshop on Nuclear Data for Fusion Reactor Technology*, Del Mar, California, 1993, pp. 3–6.
- [28] J. K. Tuli, et al., *Evaluated nuclear structure data file*, Brookhaven National Laboratory Nuclear Data Center, Brookhaven, NY (1987).
- [29] R. B. Firestone, V. S. Shirley, C. M. Baglin, S. Y. F. Chu, J. Zipkin, The 8th edition of the Table of Isotopes, in: *Proceedings of the 9th International Symposium on Capture gamma-ray spectroscopy and related topics*. V. 2, 1997.
- [30] T. Horiguchi, T. Tachibana, J. Katakura, *Chart of the Nuclides 1996*, JAERI/NDC (1996).
- [31] ICRP, *Conversion coefficients for radiological protection quantities for external radiation exposures*. ICRP publication 116, *Annals of the ICRP* 40 (2-5) (2010) 1–257. doi:<https://doi.org/10.1016/j.icrp.2011.10.001>. URL <https://doi.org/10.1016/j.icrp.2011.10.001>
- [32] ICRP, International Commission on Radiological Protection, International Commission on Radiation Units, ICRP Publication 74: *Conversion Coefficients for Use in Radiological Protection Against External Radiation*, Vol. 23, Elsevier Health Sciences, 1996.
- [33] M. Pelliccioni, *Overview of Fluence-to-Effective Dose and Fluence-to-Ambient Dose Equivalent Conversion Coefficients for High Energy Radiation Calculated Using the FLUKA Code*, *Radiation Protection Dosimetry* 88 (4) (2000) 279–297. arXiv:<https://academic.oup.com/rpd/article-pdf/88/4/279/9924648/279.pdf>, doi:[10.1093/oxfordjournals.rpd.a033046](https://doi.org/10.1093/oxfordjournals.rpd.a033046). URL <https://doi.org/10.1093/oxfordjournals.rpd.a033046>
- [34] M. Herman, Members of the Cross Sections Evaluation Working Group, *ENDF-6 Formats Manual Data Formats and Procedures for the Evaluated Nuclear Data File ENDF/B-VI and ENDF/B-VII* (6 2009). doi:[10.2172/981813](https://doi.org/10.2172/981813).
- [35] L. S. Lasdon, A. D. Waren, A. Jain, M. Ratner, Design and testing of a generalized reduced gradient code for nonlinear programming, *ACM Transactions on Mathematical Software (TOMS)* 4 (1) (1978) 34–50.
- [36] R. Q. Wright, J. L. Lucius, N. M. Greene, C. W. Craven, Jr, SUPERTOG: A program to generate fine group constants and P_n scattering matrices from ENDF/B, Tech. Rep. ORNL-TM-2679, Oak Ridge National Laboratory (1969).
- [37] Y. Kikuchi, A. Hasegawa, H. Nishimura, K. Tasaka, *Fission product fast reactor constants system of JNDC*, Tech. rep., Japan Atomic Energy Research Inst. (1976).
- [38] S. F. Mughabghab, D. I. Garber, *Neutron cross sections. Volume I. Resonance parameters*, Tech. rep., Brookhaven National Lab., Upton, NY (USA) (1973).
- [39] D. E. Cullen, *PREPRO 2019 ENDF/B Pre-processing Codes*, Tech. rep., The Nuclear Data Section, International Atomic Energy Agency (2019). URL <http://www.nds.iaea.org/ndspub/ndf/prepro/>
- [40] K. Shibata, N. Iwamoto, S. Kunieda, F. Minato, O. Iwamoto, Activation cross-section file for decommissioning of LWRs, in: *Proceedings of the 2015 Symposium on Nuclear Data*, no. JAEA-Conf 2016-004, 2015, pp. 47–52. doi:[10.11484/jaea-conf-2016-004](https://doi.org/10.11484/jaea-conf-2016-004).
- [41] K. Shibata, O. Iwamoto, T. Nakagawa, N. Iwamoto, A. Ichihara, S. Kunieda, S. Chiba, K. Furutaka, N. Otuka, T. Oh-sawa, T. Murata, H. Matsunobu, A. Zukeran, S. Kamada, J. Katakura, *JENDL-4.0: A new library for nuclear science and engineering*, *Journal of Nuclear Science and Technology* 48 (1) (2011) 1–30. arXiv:<https://doi.org/10.1080/18811248.2011.9711675>, doi:[10.1080/18811248.2011.9711675](https://doi.org/10.1080/18811248.2011.9711675). URL <https://doi.org/10.1080/18811248.2011.9711675>
- [42] M. B. Chadwick, M. Herman, P. Obložinský, et al., *ENDF/B-VII.1 nuclear data for science and technology: Cross sections, covariances, fission product yields and decay data*, *Nuclear Data Sheets* 112 (12) (2011) 2887 – 2996, special Issue on ENDF/B-VII.1 Library. doi:[10.1016/j.nds.2011.11.002](https://doi.org/10.1016/j.nds.2011.11.002). URL <http://www.sciencedirect.com/science/article/pii/S009037521100113X>
- [43] D. A. Brown, M. B. Chadwick, R. Capote, et al., *ENDF/B-VIII.0: The 8th major release of the nuclear reaction data library with CIELO-project cross sections, new standards and thermal scattering data*, *Nuclear Data Sheets* 148 (2018) 1 – 142, special Issue on Nuclear Reaction Data. doi:<https://doi.org/10.1016/j.nds.2018.02.001>. URL <https://www.sciencedirect.com/science/article/pii/S0090375218300206>
- [44] A. Plompen, et al., The Joint Evaluated Fission and Fusion nuclear data library, JEFF-3.3, Submitted to The European Physical Journal (2019).
- [45] R. A. Forrest, R. Capote, N. Otsuka, T. Kawano, A. J. Koning, S. Kunieda, J.-C. Sublet, Y. Watanabe, FENDL-3 library-summary documentation, Tech. Rep. INDC(NDS)–0628, International Atomic Energy Agency (Dec. 2012).
- [46] J.-C. Sublet, L. W. Packer, J. Kopecky, R. A. Forrest, A. J.

- Koning, D. A. Rochman, The European Activation File: EAF-2010 neutron-induced cross section library, Tech. Rep. CCFE-R (10) 05 (2010).
- [47] A. I. Blokhin, E. V. Gai, A. V. Ignatyuk, I. I. Koba, V. N. Manokhin, V. N. Pronyaev, New version of neutron evaluated data library BROND-3.1, *Yad. Reak. Konst* 2 (2) (2016) 62.
- [48] Z. G. Ge, Z. X. Zhao, H. H. Xia, Y. X. Zhuang, T. J. Liu, J. S. Zhang, H. C. Wu, The updated version of Chinese evaluated nuclear data library (CENDL-3.1), *J. Korean Phys. Soc* 59 (2) (2011) 1052–1056.
- [49] D. Rochman, A. J. Koning, J.-C. Sublet, M. Fleming, E. Bauge, S. Hilaire, P. Romain, B. Morillon, H. Duarte, S. Goriely, et al., The TENDL library: hope, reality and future, *EPJ Web Conf.* 146 (2017) 02006. doi:10.1051/epjconf/201714602006.
- [50] A. J. Koning, D. Rochman, *Modern nuclear data evaluation with the TALYS code system*, *Nuclear Data Sheets* 113 (12) (2012) 2841 – 2934, special Issue on Nuclear Reaction Data. doi:https://doi.org/10.1016/j.nds.2012.11.002. URL <http://www.sciencedirect.com/science/article/pii/S0090375212000889>
- [51] J. Taylor, *Introduction to Error Analysis, the Study of Uncertainties in Physical Measurements*, 2nd Edition, 1997.
- [52] T. Furuta, T. Sato, M. C. Han, Y. S. Yeom, C. H. Kim, J. L. Brown, W. E. Bolch, *Implementation of tetrahedral-mesh geometry in Monte Carlo radiation transport code PHITS*, *Physics in Medicine and Biology* 62 (12) (2017) 4798–4810. doi:10.1088/1361-6560/aa6b45. URL <https://doi.org/10.1088/1361-6560/aa6b45>
- [53] L. Carter, T. Crawford, T. Sato, T. Furuta, C. Choi, C. H. Kim, J. Brown, W. Bolch, P. Zanzonico, J. Lewis, PARaDIM – A PHITS-based Monte Carlo tool for internal dosimetry with tetrahedral mesh computational phantoms, *Journal of Nuclear Medicine* (06 2019). doi:10.2967/jnumed.119.229013.
- [54] H. G. Weller, G. Tabor, H. Jasak, C. Fureby, *A tensorial approach to computational continuum mechanics using object-oriented techniques*, *Comput. Phys.* 12 (6) (1998) 620–631. doi:10.1063/1.168744. URL <https://doi.org/10.1063/1.168744>
- [55] D. Schumann, J. Neuhausen, J. Eikenberg, M. Rüthi, M. Wohlmuther, P. W. Kubik, H.-A. Synal, M. V. Alfimov, G. Korschinek, G. Rugel, T. Faestermann, Radiochemical analysis of a copper beam dump irradiated with high-energetic protons, *Radiochimica Acta* 97 (7 2009). doi:10.1524/ract.2009.1585.
- [56] G. Vogin, A. Wambersie, M. Koto, T. Ohno, M. Uhl, P. Fosati, J. Balosso, ULICE WP2 working group, et al., A step towards international prospective trials in carbon ion radiotherapy: investigation of factors influencing dose distribution in the facilities in operation based on a case of skull base chordoma, *Radiation Oncology* 14 (1) (2019) 24.
- [57] G. Turk, M. Levoy, *The Stanford Bunny* (2005).
- [58] H. Si, *TetGen, a Delaunay-based quality tetrahedral mesh generator*, *ACM Trans. Math. Softw.* 41 (2) (Feb. 2015). doi:10.1145/2629697. URL <https://doi.org/10.1145/2629697>
- [59] M. J. Berger, J. S. Coursey, M. A. Zucker, ESTAR, PSTAR, and ASTAR: computer programs for calculating stopping-power and range tables for electrons, protons, and helium ions (version 1.23), Tech. rep. (1999).
- [60] C. B. Sullivan, A. A. Kaszynski, *PyVista: 3D plotting and mesh analysis through a streamlined interface for the Visualization Toolkit (VTK)*, *Journal of Open Source Software* 4 (37) (2019) 1450. doi:10.21105/joss.01450. URL <https://doi.org/10.21105/joss.01450>
- [61] B. Thomadsen, R. Nath, F. B. Bateman, J. Farr, C. Glisson, M. K. Islam, T. LaFrance, M. E. Moore, X. G. Xu, M. Yudelev, Potential hazard due to induced radioactivity secondary to radiotherapy: the report of Task Group 136 of the American Association of Physicists in Medicine, *Health physics* 107 (5) (2014) 442–460.
- [62] SCK•CEN, *BR2 - Belgian Reactor 2 US National Scientific User*

Affiliate facility User's Guide (2018).

URL <https://nsuf.inl.gov/Home/PartnerFacility/1707>